ISSN 1062-7391, Journal of Mining Science, 2019, Vol. 55, No. 1, pp. 18–22. © Pleiades Publishing, Ltd., 2019.
Russian Text © The Author(s), 2019, published in Fiziko-Tekhnicheskie Problemy Razrabotki Poleznykh Iskopaemykh, 2019, No. 1, pp. 22–28.

GEOMECHANICS

Modeling Shock Wave Processes in a Mine Opening with Permeable Barriers

V. M. Fomin[a,b]*, B. V. Postinkov[a,b], V. A. Kolotilov[a,b], V. S. Shalaev[c], Yu. V. Shalaev[c], and N. F. Florya[c]*****

[a]*Khristianovich Institute of Theoretical and Applied Mechanics, Siberian Branch, Russian Academy of Sciences, Novosibirsk, 630090 Russia*
**e-mail: fomin@itam.nsc.ru*
[b]*Novosibirsk State University, Novosibirsk, 630090 Russia*
***e-mail: b.postnikov@nsu.ru*
[c]*Shaktpozharservis Research and Production, Kemerovo, 650000 Russia*
****e-mail: florya@shps.ru*

Received December 10, 2018
Revised January 12, 2019
Accepted January 29, 2019

Abstract—The results of numerical modeling of intense shock wave propagation after explosion in a mine opening with permeable screen are presented. The problem is solved in the equilibrium non-viscous formulation without regard to chemical reactions and with averaged composition of mine air. It is shown that for a screen composed of four similar permeable barriers arranged as a labyrinth, the incoming shock wave has a strongest impact on the first barrier. As a consequence of weakening of the shock wave front on the first barrier, the rest barriers experience much less loading. In order to decrease peak loads on a load-bearing frame, it is necessary to reduce areas of flat front surfaces of metal structures.

Keywords: Shock wave, mine opening, explosion, permeable barrier.

DOI: 10.1134/S106273911901524X

INTRODUCTION

Explosion of dust–methane–air mixtures is one of the risk factors of accident initiation in coal mines; besides, large-scale accidents are practitally inevitable there [1, 2]. Understanding of the development dynamics of shock wave processes arising both at the moment of explosion, and in the course of shock-wave front passage through branched mine channels is crucial for creating effective protection instruments and procedures. Shaktpozharservis Research and Production developed the system to control mine air, rock mass and reduce explosion injurious effects [3]. The system includes a screen designed to weaken shock-wave impact on the objects to be protected, extinguish fire and abate dust and smoke [4]. The screen represents a complex consisting of four permeable barriers arranged labyrinthically at a certain distance from each other, water curtain and water curtain control unit.

Unlike the impermeable ones, permeable barriers enable to weaken shock-wave front and reduce the impact on barrier structures. Shock wave propagation modeling in mine openings is a critical task for estimating the parameters of impact on permeable barriers. Calculation of shock wave propagation from explosion in the channels with arbitrary geometry and multiphase gas atmosphere is a complex problem, in modeling it requires to take all the geometry features and physicochemical processes beyond the shock-wave front into account.

The problem on shock wave passage through the screen of permeable barriers in this paper was solved in two-dimensional approximation using equilibrium non-viscous formulation without regard to chemical reactions and with averaged composition of mine air. That allowed obtaining basic gas-dynamic parameters of shock-wave process development.

The computational domain geometry was set up on the basis of drawings of mesh barriers arranged at a similar distance from each other, in a mine opening with arch lining. The stated problem is described by a system of unsteady-state equations characterizing equilibrium non-viscous gas flow without regard to chemical reactions and considering the gas mixture integrally:

$$\frac{\partial(\phi\rho)}{\partial t} + \nabla(\rho\vec{V}) = 0, \tag{1}$$

$$\frac{\partial(\phi\rho\vec{V})}{\partial t} + \nabla(\rho\vec{V}\cdot\vec{V}) = -\nabla p + S_n, \tag{2}$$

$$\frac{\partial(\phi\rho E)}{\partial t} + \nabla(\vec{V}(\rho E + p)) = 0, \tag{3}$$

$$p = \rho\frac{RT}{M}, \tag{4}$$

$$E = C_v T, \quad C_p - C_v = R, \quad C_p = \text{const}, \tag{5}$$

$$\rho = \sum_{i=1}^{4}\alpha_i\rho_i + \sum_{m=5}^{6}\rho_m, \tag{6}$$

$$C_p = \sum_{i=1}^{4}k_i C_{p_i} + \sum_{m=5}^{6}k_m C_{p_m}, \tag{7}$$

$$S_n = -C_0 V^2, \tag{8}$$

$$C_0 = \text{const}, \tag{9}$$

$$\phi = \text{const}. \tag{10}$$

Here, ϕ is the porosity; ρ is the mixture density; ρ_i is the density of an *i*-th gas component of the mixture; ρ_m is the density of an *m*-th gas-free component of the mixture; V is the mixture velocity; p is the mixture pressure; S_n is the mixture impulse loss in porosity zone; t is the time; E is the mixture internal energy; T is the mixture temperature; R is universal gas constant; M is the mixture molar weight; C_v is the mixture heat capacity at constant volume; C_p is the mixture heat capacity at constant pressure; C_{p_i} is the heat capacity of the *i*-th gas component of the mixture at constant pressure; C_{p_m} is the heat capacity of *m*th gas-free component of the mixture at constant pressure; α_i is the volume concentration of the *i*-th gas component of the mixture; k_i is mass concentration of the *i*-th gas component of the mixture; k_m is mass concentration of the *m*-th gas-free component of the mixture; C_0 is the coefficient in medium resistance law.

The computational domain geometry is presented in Fig. 1 (L is the length of the computational domain; A is the water curtain zone; B is the width of computational domain; b is the barrier length; h is the barrier width; l is the distance between barriers I and IV). The equations of continuity (1), momentum conservation (2) and energy conservation (3) were restricted by a two-dimensional case. Ideal gas (4) with constant heat capacity (5) was taken into consideration. Accounting of water and coal dust presence was made integrally by the ratios (6) and (7). Equations (1)–(7), where $S_n = 0$ and $\phi = 1.0$ were assumed, were applied in the flow range beyond permeable barrier zone. The flow in gas-permeable area was described by the complete equation system (1)–(10), the value ϕ for barrier was taken as 0.42, which corresponded to averaged porosity characteristics of barriers of production screens.

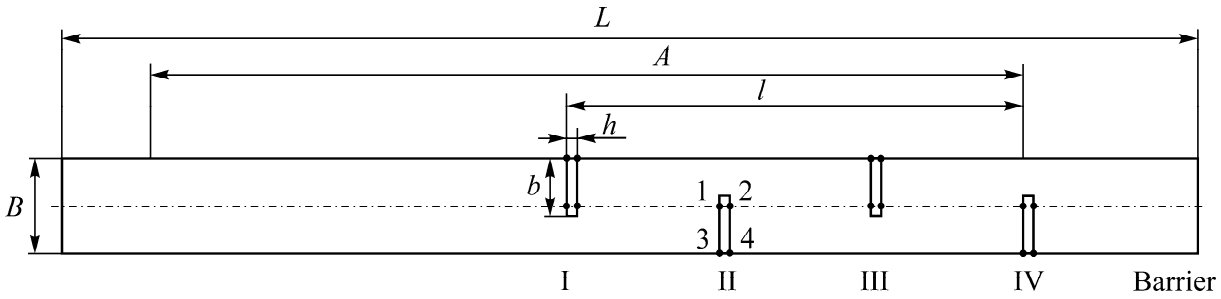

Fig. 1. Computational domain geometry. Basic geometrical ratios: $L = 65$ m; $A/L = 0.77$; $l/L = 0.4$; $b/B = 0.62$; $h/b = 0.18$. By example of barrier II, marking method is shown for computational points: along symmetry axis of steam production—1–2, on wall—3–4.

The calculations were also made with $\phi = 0$, which corresponds to the impermeable barrier. The atmospheric composition in mine opening was: CH_4—10%; O_2—19; N_2—70; Ar—1%; solid particles concentration (coal dust)—100 mg/m^3; average volume water concentration in mine opening was 0.14 l/m^3. The coefficient C_0 was chosen proceeding from the analysis of [5–8], α_i was calculated from the atmospheric composition, the remaining values from (6), (7) were chosen from the Ansys-Fluent data base of material properties with regard to [9]. Absolute pressure 0.1 MPa was set up at the initial moment of time in all computational domain, on the left boundary of opening, the absolute pressure was 0.7 MPa.

The calculations were performed by ANSYS Fluent software system. In the course of calculations shock-wave front formed, which moved left-to-right along the opening in the direction of the first barrier. The calculations ceased as the right opening boundary was reached. Density-based AUSM Flux Type solver was used by ANSYS Fluent system for solving the equations (1)–(10), the modulus for calculating the flow in porous medium, explicit scheme of the second-order accuracy, structured computational mesh consisted of 150 ths cells, the time increment was 0.3 ms.

In calculation of the screen with impermeable barriers, the shock wave moving from the left end of opening first reflects from the first barrier, at the same time, the pressure on barrier surface increases considerably (Fig. 2). The shock wave front, which passed between face plane of the first barrier and right wall of opening, keeps moving on the second barrier. Later on, shock wave reflects from the surface of the second barrier. The front of shock wave, formed as a result of multiple reflections from opening walls and backside of the first barrier, passes through the interstice between face plane of the second barrier and left wall of opening. This results in significant reduction of shock wave impact intensity to the end of opening due to multiple reflections, high molecular weight of averaged gas mixture and water curtain effect. The computational feature of permeable barriers, besides shock wave reflection from the first barrier surface, is the fact that high pressure area overcomes the barrier, and shock wave front moving to the direction of right opening end is also formed beyond the barrier. The resulting interference shock-wave pattern complicates significantly, as shock-wave front passes to the fourth permeable barrier. After shock wave front reflection, the load on the first barrier decreases considerably due to permeability. The first barrier and, to a lesser degree, the second barrier can be considered as most loaded ones. The third and fourth barriers are loaded to a significantly lesser extent due to the weakening of shock-wave front.

Since high value of flat front surface area of load-bearing elements is characteristic of load-bearing frame of screen barriers, it is required to consider calculations of pressure dynamics near impermeable $(\phi = 0)$ first barrier as the limiting case of load on load-bearing frame of screen barriers.

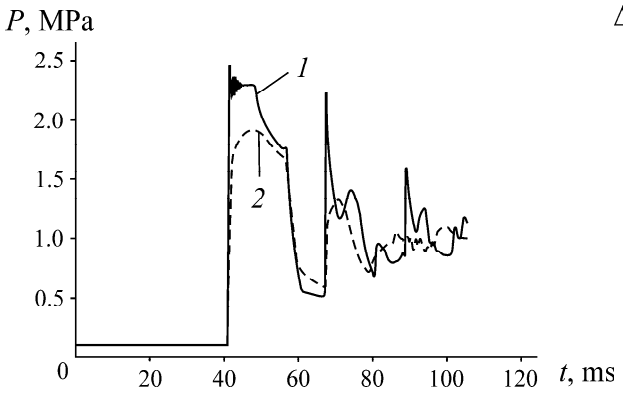

Fig. 2. Pressure–time dependence on frontal surface of the 1st barrier along the opening axis of symmetry: *1*—impermeable barrier; *2*—permeable barrier.

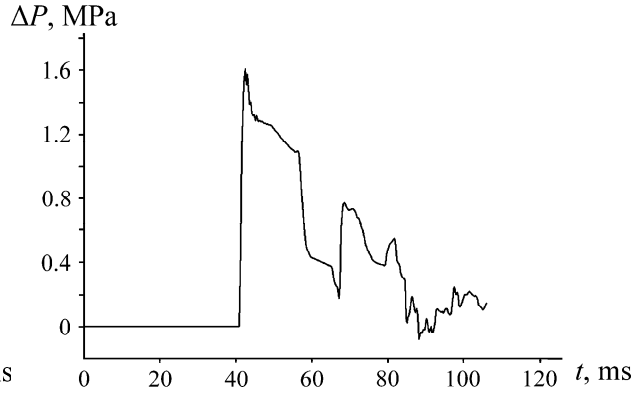

Fig. 3. Pressure difference between points 3 and 4 on first permeable barrier.

According to calculations, peak pulse pressure in this case reached 2.45 MPa (Fig. 2), pulse pressure duration after first shock wave reflection was 20 ms. Special attention must be given to impermeable angular configurations, where repeated intensive peak loads of 2.2–2.4 MPa may arise due to shock wave multiple re-reflection (Fig. 2).

Permeability of barriers significantly reduces the pressure P on front surface of the first barrier up to 1.75 MPa (Fig. 2). Passage of the permeable barrier by pressure front is a time-taking process; therefore, the pressure on backside barrier surface rises with delay, thus not compensating completely initial high pressure difference between front and back sides of the barrier.

The dependence of pressure difference ΔP between points 3 and 4 on the first permeable barrier is shown in Fig. 3. The duration of pressure difference existence on barrier in computational points, beginning from pressure jump on front surface (point 3) to the moment of pressure equalizing on front and back barrier surface (points 3, 4) is 46.8 ms, peak pressure drop is 1.61 MPa, average pressure drop at time interval indicated is 0.71 MPa.

Figure 4 presents the data on maximum pressure at the moment of shock wave reflection from front surface of barriers P_s in computational points 1 and 3, depending on their relative location $x_1 = x / l$ (x is the coordinate along opening symmetry axis, computational point 1 on front surface of the first barrier is taken as zero reference point). It is evident that shock-wave load on barriers reduces due to permeability, as the screen is passed by shock wave front.

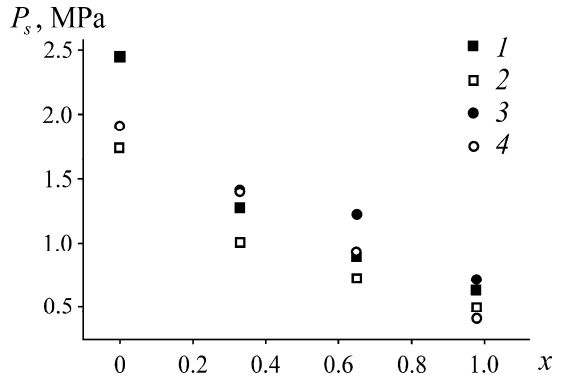

Fig. 4. Dependence of pressure on barrier location at moment of shock wave reflection from barrier front surface: *1*—impermeable barrier, point 1; *2*—permeable barrier, point 1; *3*—impermeable barrier, point 3; *4*—permeable barrier, point 3.

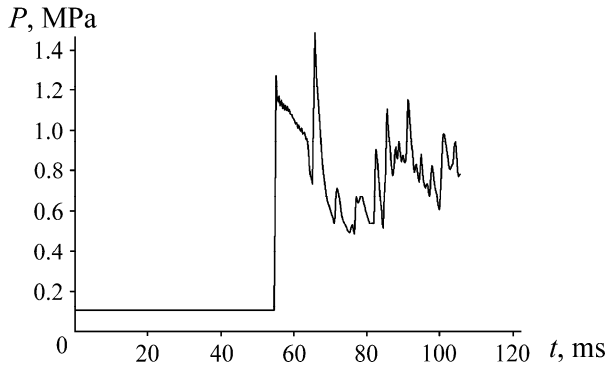

Fig. 5. Repeated pressure peak on second impermeable barrier.

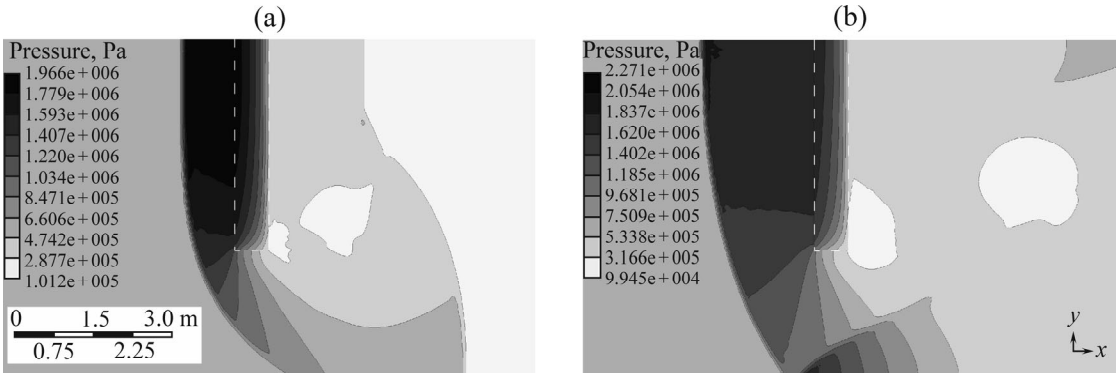

Fig. 6. Pressure field. Displacing area of anomalous pressure near right opening wall. Time from the beginning of computations: (a) 47.0 ms; (b) 52.5 ms.

Occurrence of areas with anomalous gas-dynamic parameters is typical of shock-wave processes with time. Figure 5 shows the appearance of repeated, more intensive pressure peak on symmetry axis of the second barrier for computation with impermeable walls, where this effect is most evident. High pressure areas may arise in the opening space for short time periods. After reflection from the first permeable barrier, shock wave reaches the right wall of opening, the area of anomalously high pressure up to 2.3 MPa displacing along the right wall of opening in opposite direction arises as a result of repeated reflection (Fig. 6). Time of the area existence is insignificant and does not exceed 10 ms.

CONCLUSIONS

In the studied screen configurations incident shock wave exerts the strongest power impact on the first barrier. As the shock-wave front on this barrier is weakened, the remaining barriers are loaded to a considerably lesser extent. An increase in the first barrier permeability allows more uniform distribution of pressure from incident shock wave between screen barriers. After reflection from the barrier, a high pressure area is formed on its surface, beyond the front of reflected shock wave. The pressure in that area exceeds the pressure beyond the front of incident shock wave by several times. This is one of the key effects in developing and designing perspective permeable barriers. To decrease peak loads on a load-bearing frame, it is required to reduce areas of flat front surfaces and avoid three-dimensional semi-closed configurations for the prevention of cumulative pressure growth.

REFERENCES

1. Kurlenya, M.V. and Skritsky, V.A., Methane Explosions and Causes of Their Origin in Highly Productive Sections of Coal Mines, *J. Min. Sci.*, 2017, vol. 53, no. 5, pp. 71–78.
2. Abramov, V.V., Brilev, M.G., and Abramov, O.V., Is It Possible to Avoid Large-Scale Accidents in Coal Mines?, *Bezop. Trud. Prom*., 2018, no. 7, pp. 48–53.
3. Shalaev, V.S., Shalaev, A.V., and Shalaev, Yu.V., RF patent no. 2400633, *Byull. Izobret.*, 2010, no.27.
4. Shalaev, V.S., Shalaev, Yu.V., and Florya, N.F., Explosion Protection Instruments for Openings of Coal Mines and Their Testing, *Bezop. Trud. Prom*., 2015, no. 5, pp. 46–49.
5. Sheidegger, A.E., *Fizika techeniya zhidkostei cherez poristye sredy* (Physics of Fluids Flow through Porous Media), Moscow: Gos. Nauch. Tekh. Izd. Neft. Gorn. Lit., 1960.
6. Belov, S.V., *Poristye pronitsaemye materialy* (Porous Permeable Materials), Moscow: Metallurgiya, 1987.
7. Mironov, S.G., Kolotilov, V.A., and Maslov, A.A., Experimental Investigation of Filtration Properties of Highly Porous Cell Materials, *Teplofiz. Aeromekh.,* 2015, vol. 22, no. 5, pp. 599–607.
8. Postnikov, B.V., Lomanovich, K.A., and Ponomarenko, R.A., Influence of Gas-Permeable Materials with Changeable Porosity on Separated Flow in Supersonic Flow of Straight Bench, *Teplofiz. Aeromekh,* 2018, vol. 25, no. 2, pp. 199–205.
9. Kikoin, I.K., *Tablitsy fizicheskikh velichin* (Tables of Physical Values), Moscow: Atomizdat, 1976.